NANO LETTERS
Cite This: Nano Lett. 2018, 18, 2054−2059
Letter
pubs.acs.org/NanoLett

Large-Area High-Performance Flexible Pressure Sensor with Carbon Nanotube Active Matrix for Electronic Skin

Luca Nela,[⊥] Jianshi Tang,*[,⊥] Qing Cao, George Tulevski, and Shu-Jen Han*

IBM Thomas J. Watson Research Center, Yorktown Heights, New York 10598, United States

Supporting Information

ABSTRACT: Artificial "electronic skin" is of great interest for mimicking the functionality of human skin, such as tactile pressure sensing. Several important performance metrics include mechanical flexibility, operation voltage, sensitivity, and accuracy, as well as response speed. In this Letter, we demonstrate a large-area high-performance flexible pressure sensor built on an active matrix of 16 × 16 carbon nanotube thin-film transistors (CNT TFTs). Made from highly purified solution tubes, the active matrix exhibits superior flexible TFT performance with high mobility and large current density, along with a high device yield of nearly 99% over 4 inch sample area. The fully integrated flexible pressure sensor operates within a small voltage range of 3 V and shows superb performance featuring high spatial resolution of 4 mm, faster response than human skin (<30 ms), and excellent accuracy in sensing complex objects on both flat and curved surfaces. This work may pave the road for future integration of high-performance electronic skin in smart robotics and prosthetic solutions.

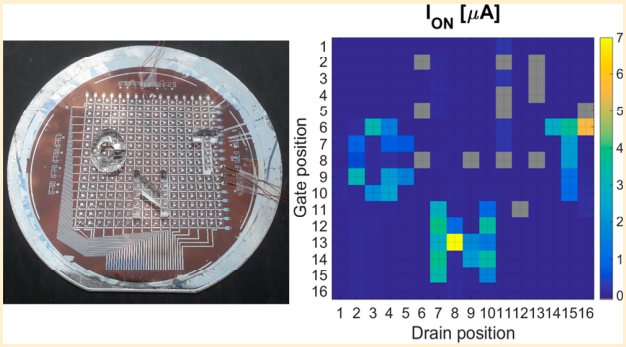

KEYWORDS: *Flexible pressure sensor, electronic skin, CNT TFTs, active matrix, flexible electronics*

The ability of sensing tactile pressure from arbitrarily shaped objects using an integrated electronic interface is a key element for the development of smart robotics and prosthetic solutions.[1−5] For the applications of artificial electronic skin, several transduction mechanisms, including capacitance/resistance variation or piezoelectric and piezotronic effect,[6−12] have been investigated. A critical challenge in making resistive electronic skins has been the realization of high-performance large-area active matrix of flexible thin-film transistors (TFTs). For this purpose, various materials, such as organic polymers,[13−16] carbon nanotubes (CNTs),[17−21] and semiconductor nanowires,[22] have been extensively explored to build flexible pressure sensors. Each of those materials has its own advantages and challenges for flexible electronics. For example, organic TFT-based active matrices with high device yields over large areas have been reported; however, they usually suffer from relatively low mobility and require a large voltage range (e.g., tens of volts) to operate.[13−16] In comparison, CNT TFTs could offer exceptional performance in terms of higher mobility and current density, superior environmental stability, and excellent mechanical robustness.[19,23−25] To build practical CNT-based flexible pressure sensors, several important metrics need to be considered together, such as TFT performance (including mobility, on/off ratio, yield), pressure sensitivity, and accuracy, as well as response speed. Due to process limitations on flexible substrates (e.g., substrate cleanliness, process temperature, lithography resolution, etc.), it remains challenging to build large-area flexible pressure sensors that are capable to accurately sense complex objects with high sensitivity, low defects, and fast response speed, especially on a curved surface. Previous demonstrations of such pressure sensors either featured relatively low TFT performance that required large voltage ranges to operate (especially those made by printing technique)[20,21] or showed a considerable number of defective pixels that may be caused by low device yield or poor sensing accuracy.[18,19] In this work, we have demonstrated a 4 inch high-performance flexible pressure sensor based on an active matrix of 16 × 16 CNT TFTs. By tuning the TFT performance, the integrated pressure sensor can operate within a small voltage range of 3 V, compatible with most digital interfaces. With a high spatial resolution down to a single pixel of 4 mm, it has also shown fast response time of less than 30 ms and high accuracy in sensing complex objects on both flat and curved surfaces.

To start, CNT TFTs were fabricated on a flexible 75 μm-thick polyimide film (w), which was prelaminated on a silicon handling wafer using polydimethylsiloxane (PDMS) and epoxy. Figure 1a illustrates the device structure and schematic of fabrication process flow. In brief, local bottom gates (along with 16 gate lines for probing), consisting of 2 nm titanium (Ti)/50 nm palladium

Received: January 5, 2018
Revised: February 8, 2018
Published: February 14, 2018

DOI: 10.1021/acs.nanolett.8b00063
Nano Lett. 2018, 18, 2054−2059

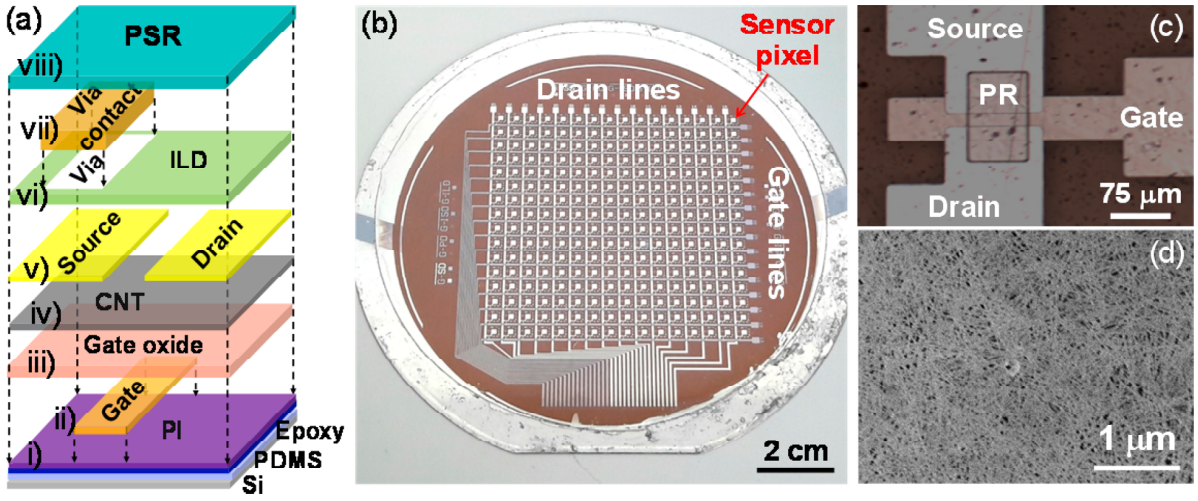

Figure 1. Fabrication of the active matrix of CNT TFTs for flexible pressure sensor. (a) Schematic of the process flow for the flexible pressure sensor: (i) lamination of poly I) film on a Si handling wafer; (ii) back gate patterning by photolithography and metal deposition; (iii) bilayer gate oxide deposition by ALD; (i) source/drain patterning and then channel definition by etching; (vi) interlayer dielectric (ILD) deposition and pad opening on top of source pads; (v) via contact formation by conductive ink printing; (viii) lamination of pressure-sensitive rubber (PSR). (b) Photograph of a complete active matrix of 16 × 16 CNT TFTs. Each white square (indicated by the red arrow) is a pixel in the pressure sensor. (c) Microscope image of a CNT TFT. The photoresist (PR) mask is used to define the TFT channel with a dimension of W_{ch}/L_{ch} = 75 μm/20 μm. (d) SEM image of the deposited high-density CNT thin film.

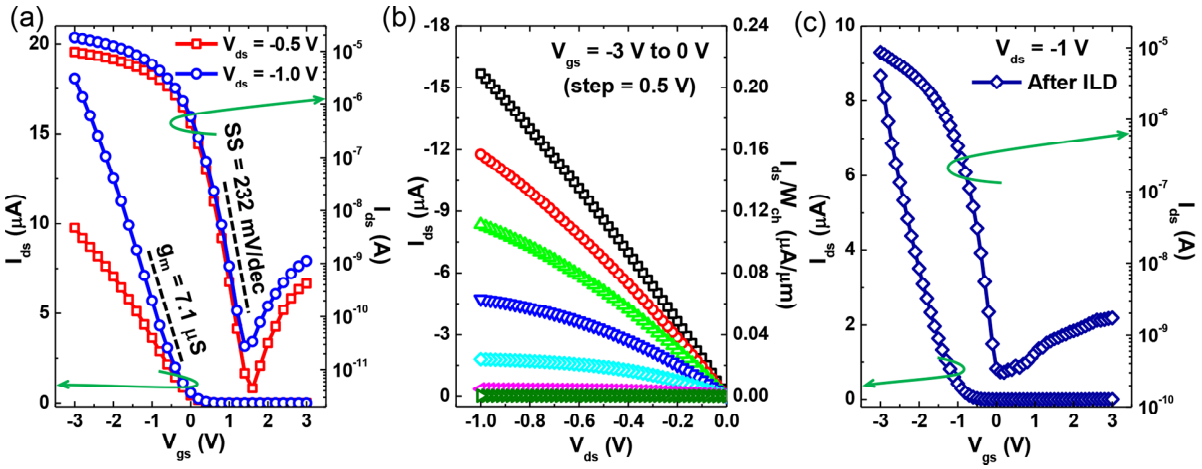

Figure 2. Electrical characterizations of CNT TFT. (a) I_{ds}–V_{gs} transfer curves of a typical CNT TFT at V_{ds} = −0.5 and −1 V in linear (left axis) and logarithmic (right axis) scales. The extracted transconductance and subthreshold slope at V_{ds} = −1 V are g_m = 7.1 μS and SS = 232 mV/dec, respectively. (b) I_{ds}–V_{ds} output curves of the CNT TFT at V_{gs} ranging from −3 to 0 V (from top to bottom). (c) I_{ds}–V_{gs} transfer curves V_{ds} = −1 V in linear (left axis) and logarithmic (right axis) scales after the ILD deposition, which negatively shifts the threshold voltage to minimize leakage during pressure sensing.

(Pd)/1 nm Ti, were first defined by standard photolithography and metal deposition, followed by atomic layer deposition (ALD) of 40 nm Al_2O_3/20 nm HfO_2 at 150 °C as the gate dielectric. The equivalent relative dielectric constant was estimated to be ε_r = 7.26 from capacitance measurements on a control sample with the same stack of ALD oxides. High-density poly (with a high semiconducting purity >99.99%) were deposited on the sample surface through standard drop-casting method.[25] The deposited CNT random network showed a relatively uniform density over the 4 inch sample area (see Supporting Information S1). Source/drain contacts (a) with a stack of 0.2 nm Ti/70 nm Pd/2 nm Ti were then defined by another photolithography and e-beam evaporation. After that, CNT TFT channels with length of L_{ch} = 20 μm and width of W_{ch} = 75 μm were defined using photolithography followed by oxygen plasma etching. To protect the CNT TFTs and also adjust the threshold voltage, the sample was passivated with 20 nm-thick Al_2O_3 by ALD at 150 °C and then 1.5 μm-thick photoresist (A), which also served as the interlayer dielectric (ILD). Via contacts through the ILD were made to each source pad through pad opening lithography and etching. Finally, a commercially available ZOFLEX ZL45.1 pressure-sensitive rubber (PSR), which has a drastic pressure response,[26] was laminated on top of the active matrix. After the device fabrication, the polyimide substrate was peeled from the silicon handling wafer, yielding a flexible pressure sensor with 16 × 16 pixels. Figure 1b displays the complete active matrix with 256 CNT TFTs, and Figure 1c shows the microscope image of an individual TFT. The high-density CNT thin film in the channel

DOI: 10.1021/acs.nanolett.8b00063
Nano Lett. 2018, 18, 2054−2059

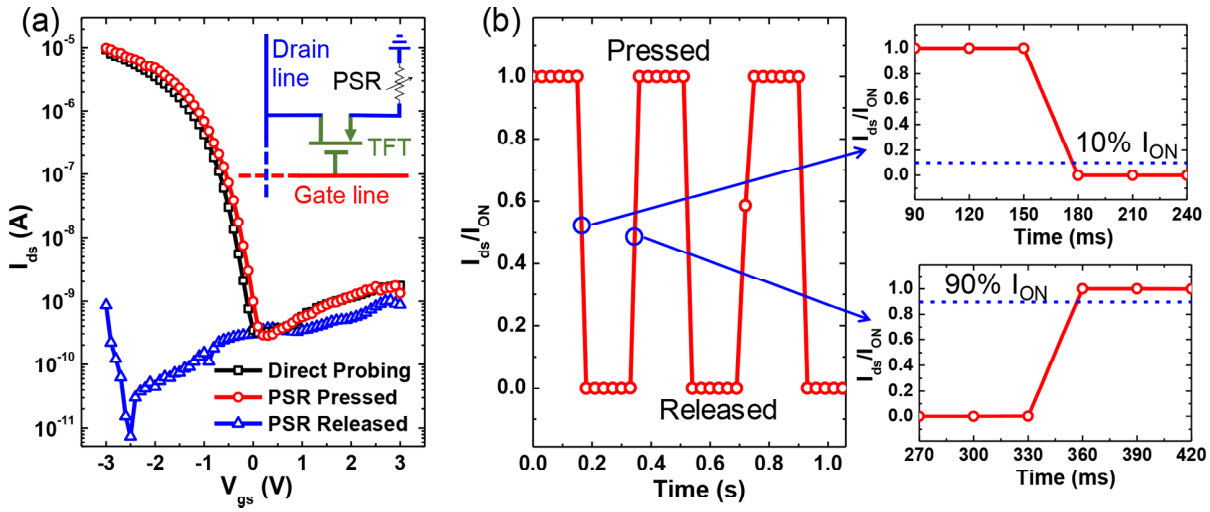

Figure 3. Pressure response and dynamics of a single pixel. (a) I_{ds}–V_{gs} transfer curves at V_{ds} = −1 V for an individual pixel when directly probing through the source pad (black), when the PSR is pressed (red), and when the PSR is released (blue), respectively. The pressure applied is estimated to be 5 kPa. It is also shown that the PSR does not affect the TFT ON current. The inset shows the circuit diagram for a single pixel in the pressure sensor. (b) Time-resolved measurement of the sensor response between pressed and released states. The measurement is carried out by biasing the TFT with V_{gs} = −3 V and V_{ds} = −1 V, while a weight is repeatedly dropped and lifted on the PSR. The time resolution of the measurement equipment is 30 ms. The zoomed insets are used to extract the fall time when the weight is lifted (top panel) and the rise time when the weight is dropped (bottom panel).

region was verified by scanning electron microscope (SEM), as shown in Figure 1d. The typical CNT length is around 1 μm, and the tube density is about 100 tubes/μm^2.

To characterize the CNT TFT performance in the active matrix, Figure 2a,b shows the I_{ds}–V_{gs} transfer curve and corresponding I_{ds}–V_{ds} output curves for a representative pixel, respectively. The TFT shows a high ON/OFF ratio (I_{ON}/I_{OFF}) over 10^5, thanks to the ultrahigh purity of semiconducting tube used in this work. The ON current density, I_{ON}/W_{ch} = 0.21 μA/μm at a small V_{ds} of −1 V, is also among the highest reported values reported for flexible CNT TFTs with similar channel length, and it can be further improved by nearly two orders of magnitude when scaling down the channel length as reported in our earlier work.[25] To estimate the carrier mobility, the gate capacitance C_{ox} can be first calculated using the parallel plate model as $C_{ox} = \varepsilon_0\varepsilon_r/t_{ox}$ (upper limit), considering the high density of the CNT network and the relatively thick gate oxide (oxide thickness is larger than tube spacing).[27] Given the extracted transconductance of g_m = 7.1 μS at V_{ds} = −1 V, the field-effect carrier mobility is estimated to be $\mu = \frac{g_m L_{ch}}{V_{ds} C_{ox} W_{ch}}$ = 17.6 cm^2/(V·s). This value falls in the typical range of literature-reported mobility (1–100 cm^2/(V·s)) for flexible CNT TFTs,[17−19] and it is much higher than those of organic TFTs.[13−15,28] The subthreshold slope is extracted to be SS = 232 mV/dec, even with a relatively thick gate oxide stack.

When integrating CNT TFTs in the active matrix for pressure sensor, it is important to make sure the inactivated pixels (usually biased with V_{gs} = 0 V) are fully turned off in order to minimize leakage current and avoid crosstalk. This can be readily implemented by adjusting the threshold voltage V_T through doping, which can be achieved by ALD oxide passivation as reported previously.[25] Here, we passivated the fabricated CNT TFTs with a bilayer ILD consisting of 20 nm-thick Al_2O_3 and 1.5 μm-thick photoresist. Figure 2c shows the I_{ds}–V_{gs} transfer curves V_{ds} = −1 V in linear (left axis) and logarithmic (right axis) scales after the ILD deposition, which negatively shifts V_T from ∼0 V to about −1 V, reducing the TFT OFF state leakage at V_{gs} = 0 V by nearly three orders of magnitude. The fabricated CNT TFTs across the 4 inch sample area showed a very high device yield (almost 99%) and relatively good uniformity in terms of ON current I_{ON} and also I_{ON}/I (see Supporting Information S2). Overall, the adjusted V_T, along with the relatively small SS and device variation, enables the CNT TFT active matrix to operate within a small voltage range of 3 V, which allows the entire pressure sensor system to be easily driven and interfaced with most commercial digital circuits.

To characterize the integrated pressure sensor, we first demonstrated the pressure sensing function of an individual pixel and further investigated the response speed. In this measurement, the grounded PSR was connected to the source pad of the CNT TFT, and the drain and gate lines were biased separately, as shown in Figure 3a. When pressed ($P \approx 5$ kPa), the PSR exhibited a very low resistance (<0.1 Ω),[26] so the TFT was turned on with a small parasitic PSR resistance in the source terminal (it is noted that the PSR does not affect the TFT ON state). When released ($P \approx 0$), the PSR resistance became very high (>30 MΩ) so the TFT was switched off. The transition between the high and low resistance states was abrupt with a threshold pressure around ∼1 k , the PSR response can be considered as "digital". At a constant gate bias of V_{gs} = −3 V, the I_{ds} ratio between pressed and released states is above 10^4, giving rise to a large sensing margin and signal-to-noise ratio for reading. It also helps accurately sense complex objects over a large area using this integrated pressure sensor. To estimate the response time, we alternated the above press and release processes under constant biases of V_{gs} = −3 V and V_{ds} = −1 V and recorded I_{ds} over time in Figure 3b. As we can see, both the fall time (defined as when I_{ds} drops to 10% of I_{ON}) and the rise time (when I_{ds} reaches 90% of I_{ON}) are less than 30 milliseconds (ms), whose measurements are actually limited by the instrument that has a minimum sampling interval of 30 ms. Such response speed is already much faster than

DOI: 10.1021/acs.nanolett.8b00063
Nano Lett. 2018, 18, 2054−2059

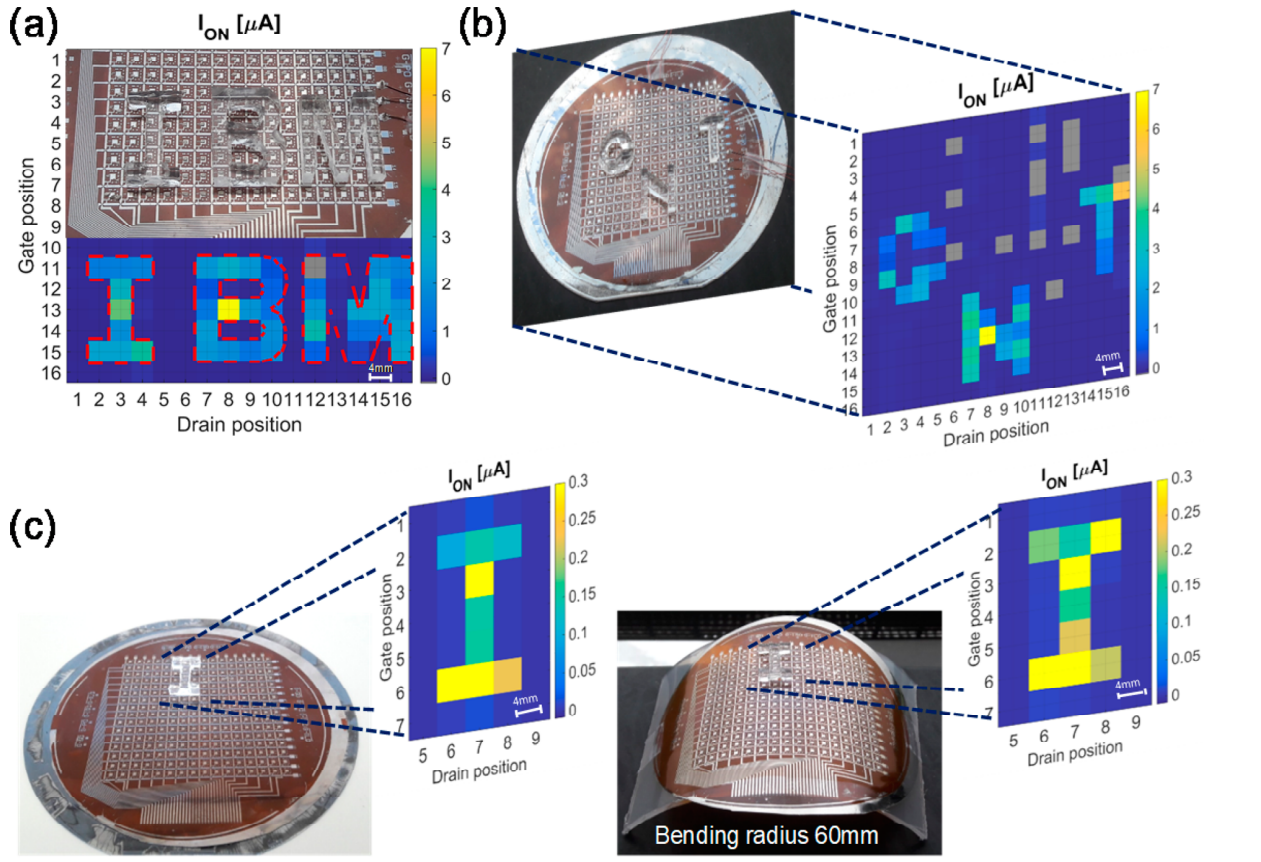

Figure 4. Pressure mapping of complex objects on flat and curved surfaces. (a) Current mapping of the CNT TFT active matrix showing the pressure sensing of "IBM" logo made by PDMS. (b) Current mapping for the pressure sensing of word "CNT" made by PDMS. The defective pixels are la led in gray color. (c) Comparison of pressure sensing on flat (left) and curved (right) surfaces with a bending radius of 60 mm. In both mappings, the pressure applied is ~6.8 kPa.

human skin (t l response time is ~0.2 s),[29] and, to the best of our knowledge, it is the fastest reported for similar resistive electronic skin sensors.[13,22] It should be noted that sensor response time is not limited by the CNT TFT switching speed itself (over 1 MHz, see Supporting Information S3) but rather the mechanical response of the PSR.

To demonstrate the ability of "electronic skin" to sense complex objects with arbitrary shape, stamps of letters carved from 5 mm-thick PDMS layer were used to apply a constant pressure (~6.8 kPa) on the PSR. Figure 4a,b shows the demonstrations with "IBM" logo and word "CNT" (plotted as current mapping of the active matrix), where a high sensing accuracy down to about single pixel resolution was achieved. The large current ratio between the activated pixels under these objects (a) and the inactivated ones (average $I_{ds} \approx 16$ nA) makes it easy to illustrate the shape of applied weights as resembled by the current mapping. The spatial resolution, roughly 6.35 pixels per inch (ppi), is limited by the pixel size of 4 mm in the current layout, and it can be readily improved if required by specific applications since each TFT channel here only occupies a small area of 20 μm by 75 μm. In this experiment, the CNT TFT active matrix with 256 pixels was scanned sequentially through the gate and drain lines, during which sensing biases of $V_{gs} = -3$ V and $V_{ds} = -1$ V were applied to the selected pixel, while the other gate/drain lines that were not activated were grounded to avoid crosstalk. This is also to mimic the case when interfacing with demultiplexers for the gate and drain lines in practical a [15] For this purpose, it is again critical to carefully tune the V_T of CNT TFT to below 0 V so that all the inactivated pixels on the same drain line as the selected pixel are turned off ($I_{ds} < 1$ nA) with grounded gate lines ($V_{gs} = 0$ V). It should be noted that the high I_{ON}/I_{OFF} ratio and carefully tuned V_T in our CNT TFTs allow the integrated pressure sensor to tolerate a small hysteresis in the TFT (see Supporting Information S4).

Furthermore, in order to better mimic the functionality of soft human skin, it is important to demonstrate the pressure sensing of comple lso curved surface, which however has been rarely demonstrated in the literature.[14 19] In our earlier work, we have shown that the flexible CNT TFTs fabricated in similar fashion exhibited excellent flexibility and robustness with bending radius down to 5 mm (curvature similar to human fingers).[25] Such feature allows our flexible pressure sensor to work on a curved surface as well, which is again crucial for practical applications. Figure 4c plots the current mappings to sense the same object (letter "I") on both flat and curved (w) surfaces, showing similar sensing results. The single-pixel accuracy of pressure mapping is fully retained on curved surface. The large current contrast between the activated pixels and the inactivated ones is also preserved, indicating no structural damage to the CNT TFT during bending. It is therefore suggested that our flexible pressure sensor could be

DOI: 10.1021/acs.nanolett.8b00063
Nano Lett , 18, 2054−2059

used to sense more complex objects on an arbitrary curved surface.

In conclusion, we have demonstrated a fully integrated high-performance flexible pressure sensor based on a CNT TFT active matrix with 16 × 16 pixels spanning over a 4 inch area. Using a semiconductor-enriched CNT solution, we have fabricated the flexible active matrix with a very high yield and good uniformity. This has enabled the integrated pressure sensor to successfully sense complex objects with high accuracy down to single-pixel spatial resolution of 4 mm while operating within a small voltage range of 3 V. It is found that the pressure response time is less than 30 ms, which is much faster than human skin. Furthermore, we have demonstrated that the flexible pressure sensor functioned well on both flat and curved surfaces without compromising its sensing accuracy. Our work provides a robust approach to integrate CNTs in high-performance pressure sensor for future applications toward practical electronic skin, which will likely need to be both highly flexible (with even smaller bending radius) and stretchable (to accommodate elongation and strain). With the ability to build high-speed flexible complementary integrated circuits using CNT TFTs,[25] it is therefore promising to further integrate control circuits and other electronic components on the same flexible substrate to realize more functionalities.

Methods. *CNT TFTs Fabrication.* CNT TFTs were fabricated on flexible poly (DuPont Kapton 300HN), which were prelaminated on a silicon wafer using a bila 10:1 polydimethylsiloxane (PDMS) and standard hardware store epoxy. The PDMS and epoxy layers were spin-coated at 2000 and 4000 rpm for 60 s, respectively, to achieve flat surface. To maintain a strong bonding and avoid the polyimide deformation when heated, the PDMS and Kapton surfaces were functionalized with a self-assembled monolayer (SAM) of MPTMS ((3-mercaptopropyl)trimethoxysilane from Sigma-Aldrich).[30] Standard photolithography process was used to first pattern the local back gates, followed by e-beam evaporation of Ti/Pd/Ti stack and then liftoff. The gate oxide stack consisted of 40 nm Al_2O_3/20 nm HfO_2 by ALD at 150 °C. The HfO_2 layer was critical to prevent the attack from photoresist developer (A) on Al_2O_3. High-density CNT random network was then deposited on the sample by a standard drop-casting method using a polymer-sorted highly purified CNT solution (semiconducting purity > 99.99%).[25] To increase the density and uniformity of the deposited CNT film, the HfO_2 surface was precoated with a SAM of chloro(dimethyl)octadecylsilane (from Sigma-Aldrich). The receiving substrate was then thoroughly rinsed with toluene and isopropanol. After that, source/drain metal contacts were defined by photolithography and e-beam evaporation of Ti/Pd/Ti. Finally, another photolithography step was used to define the TFT channel regions. CNTs outside the channel region were etched by oxygen plasma.

Pressure Sensor Integration. After CNT TFTs fabrication, an interlayer dielectric (ILD) consisting of 20 nm-thick ALD Al_2O_3 and 1.5 μm-thick photoresist (AZ5214) was deposited to protect and passivate the TFTs. The oxide layer was used to tune the threshold voltage[25] and, at the same time, to reduce the water permeation to the CNT channel.[31] Via openings on top of source pads were then defined by photolithography, and the Al_2O_3 layer inside the openings was etched by buffered oxide etchant (BOE). Via contacts were made by printing silver chloride (AgCl) conductive ink (a 160 μm thick) on the source pads using an inject printer. After that, the commercially available ZOFLEX ZL45.1 PSR layer was laminated on top, and the AgCl conductive ink was bonded to the bottom surface of the PSR to ensure good contacts with the source pads. The top surface of the PSR was coated with silver paste to serve as a common ground for electrical testing.

Instrumentation. CNT TFTs were measured at room temperature on a manual probe station connected to an Agilent 4156C Precision Semiconductor Parameter Analyzer. The time response of CNT TFTs was measured with a Keysight InfiniiVision MSOX6004A Mixed Signal Oscilloscope. The Raman spectra were acquired with a LabRAM ARAMIS micro Raman under the excitation of a 532 nm laser.

■ ASSOCIATED CONTENT

Supporting Information

The Supporting Information is available free of charge on the ACS Publications website at DOI: 10.1021/acs.nanolett.8b00063.

Raman spectra of the deposited CNT random network; color mappings of TFT ON current and ON/OFF ratio in the active matrix; TFT time response characterizations at different frequencies; hysteresis in CNT TFT (PDF)

■ AUTHOR INFORMATION

Corresponding Authors

*E-mail: jtang@us.ibm.com.
*E-mail: sjhan@us.ibm.com.

ORCID

Jianshi Tang: 0000-0001-8369-0067

Author Contributions

⊥L.N. and J.T. contributed equally to this work.

Notes

The authors declare no competing financial interest.

■ ACKNOWLEDGMENTS

The authors would like to acknowledge the Erasmus program for the financial support. The authors also acknowledge Heike Riel and Zachary Lemnios for management support.

■ REFERENCES

(1) Hammock, M. L.; Chortos, A.; Tee, B. C. K.; Tok, J. B. H.; Bao, Z. *Adv. Mater.* **2013**, *25*, 5997−6038.
(2) Bauer, S.; Bauer-Gogonea, S.; Graz, I.; Kaltenbrunner, M.; Keplinger, C.; Schwödiauer, R , *26*, 149−162.
(3) Dahiya, R , P.; Valle, M.; Cheng, G.; Lumelsky, V. J. *IEE* **13**, *13*, 4121−4138.
(4) W , 1500169.
(5) Zang, Y.; Zhang, F.; Di, C.; Zhu, D. *Mater. Horiz.* **2015**, *2*, 140−156.
(6) Fan, F. R.; Lin, L.; Zhu, G.; Wu, W.; Zhang, R.; Wang, Z. L. *Nano Lett.* **2012**, *12*, 3109−3114.
(7) Mannsfeld, S. C. B.; Tee, B. C.-K.; Stoltenberg, R. M.; Chen, C. V. H.-H.; Barman, S.; Muir, B. V. O.; Sokolov, A. N.; Reese, C.; Bao, Z. *Nat. Mater.* **2010**, *9*, 859−864.
(8) Lipomi, D. J.; Vosgueritchian, M.; Tee, B. C.-K.; Hellstrom, S. L.; Lee, J. a.; Fox, C. H.; Bao, Z. *Nat. Nanotechnol.* **2011**, *6*, 788−792.
(9) Kwon, D.; Lee, T.-I.; Shim, J.; Ryu, S.; Kim, M. S.; Kim, S.; Kim, T.-S.; Park, I. *ACS Appl. Mater. Interfaces* **2016**, *8*, 16922−16931.
(10) Gong, S.; Schwalb, W.; Wang, Y.; Chen, Y.; Tang, Y.; Si, J.; Shirinzadeh, B.; Cheng, W. *Nat. Commun.* **2014**, *5*, 3132.
(11) Schwartz, G.; Tee, B. C. K.; Mei, J.; Appleton, A. L.; Kim, D. H.; Wang, H.; Bao, Z. *Nat. Commun.* **2013**, *4*, 1859.

DOI: 10.1021/acs.nanolett.8b00063
Nano Lett. 2018, 18, 2054−2059

(12) Tian, H.; Shu, Y.; Wang, X.-F.; Mohammad, M. A.; Bie, Z.; Xie, Q.-Y.; Li, C.; Mi, W.-T.; Yang, Y.; Ren, T.-L. *Sci. Rep.* **2015**, *5*, 8603.
(13) Someya, T.; Sekitani, T.; Iba, S.; Kato, Y.; Kawaguchi, H.; Sakurai, T. *Proc. Natl. Acad. Sci. U. S. A.* **2004**, *101*, 9966−9970.
(14) Someya, T.; Kato, Y.; Sekitani, T.; Iba, S.; Noguchi, Y.; Murase, Y.; Kawaguchi, H.; Sakurai, T. *Proc. Natl. Acad. Sci. U. S. A.* **2005**, *102*, 12321−12325.
(15) Someya, T.; Sekitani, T.; Iba, S.; Kato, Y.; Sakurai, T.; Kawaguchi, H. *Mol. Cryst. Liq. Cryst.* **2006**, *444*, 13−22.
(16) Kaltenbrunner, M.; Sekitani, T.; Reeder, J.; Yokota, T.; Kuribara, K , T.; Drack, M.; Schwödiauer, R.; Graz, I.; Bauer-Gogonea, S.; Bauer, S.; Someya, T. *Nature* **2013**, *499*, 458−463.
(17) Endoh, H. *J. Photopolym. Sci. Technol.* **2015**, *28*, 349−352.
(18) Takahashi, T.; Takei, K.; Gillies, A , R , A **11**, *11*, 5408−5413.
(19) W , C.; Hwang, D.; Yu, Z.; Takei, K.; Park, J.; Chen, T.; Ma, B.; Javey, A , *12*, 899−904.
(20) Yeom, C.; Chen, K.; Kiriya, D.; Yu, Z.; Cho, G.; Javey, A. *Adv. Mater.* **2015**, *27*, 1561−1566.
(21) Lee, W.; Koo, H.; Sun, J.; Noh, J.; Kwon, K.-S.; Yeom, C.; Choi, Y.; Chen, K.; Javey, A.; Cho, G. *Sci. Rep.* **2016**, *5*, 17707.
(22) Takei, K llies, A. G.; Leu, P. W.; Fearing, R , A. *Nat. Mater.* **2010**, *9*, 821−826.
(23) Ha, T.; Kiriya, D.; Chen, K.; Javey, A. *ACS Appl. Mater. Interfaces* **2014**, *6*, 8441−8446.
(24) Cai, L.; Wang, C. *Nanoscale Res. Lett.* **2015**, *10*, 320.
(25) Tang, J.; Cao, Q.; Tulevski, G. S.; Jenkins, K. A.; Nela, L.; Farmer, D. B.; Han, S.-J. *Nat. Electron.* **2018**, in press DOI: 10.1038/s41928-018-0038-8.
(26) ZOFLEX ZL45.1 Pressure-Activated Conductive Rubber Sheets. http://www.rfmicrolink.com/ZOFLEXZL451.pdf (accessed Feb 8, 2018).
(27) Cao, Q.; Xia, M.; Kocabas, C.; Shim, M.; Rogers, J. A.; Rotkin, S. V. *Appl. Phys. Lett.* **2007**, *90*, 023516.
(28) K Iba, S.; Teramoto, R.; Sekitani, T.; Someya, T.; Kawaguchi, H.; Sakurai, T. *Appl. Phys. Lett.* **2004**, *84*, 3789−3791.
(29) Lele, P. P.; Sinclair, D. C.; Weddell **1954**, *123*, 187−203.
(30) Hoang, M. V.; Chung, H.-J.; Elias, A. L. *J. Micromech. Microeng.* **2016**, *26*, 105019.
(31) Kim, W.; Javey, a.; Vermesh, O.; Wang, O.; Li, Y. M.; Dai, H. J. *Nano Lett.* **2003**, *3*, 193−198.

DOI: 10.1021/acs.nanolett.8b00063
Nano Lett , 18, 2054−2059